

Article

On the Response of Zhejiang Coastal Waters to 12 Typhoons from 2011 to 2015

Yunhe Pan ¹, Anzhou Cao ^{1,*} , Yuqian Wu ¹, Shiming Lu ¹, Luteng Fan ² and Peiliang Li ^{1,3}

¹ Ocean College, Zhejiang University, Zhoushan 316021, China; 21934020@zju.edu.cn (Y.P.); 22034120@zju.edu.cn (Y.W.); 21934015@zju.edu.cn (S.L.); lipeiliang@zju.edu.cn (P.L.)

² Zhoushan Technology Exchange and Entrepreneurship Service Center, Zhoushan 316012, China; fanlut@hotmail.com

³ Hainan Institution of Zhejiang University, Sanya 572025, China

* Correspondence: caoanzhou@zju.edu.cn

Abstract: Based on the hybrid coordinate ocean model (HYCOM) reanalysis data, the dynamical and thermal response of Zhejiang coastal waters to 12 typhoons from 2011 to 2015 was studied, and the relationship between the oceanic response and typhoon characteristics was analyzed. The HYCOM reanalysis data were validated by satellite-observed sea surface temperature data. Results show that all the 12 typhoons caused near-inertial waves, sea surface cooling and seafloor warming, but significant differences existed among them. Based on statistics, it was found that the domain-averaged near-inertial kinetic energy and seafloor warming are significantly correlated with the typhoon's maximum wind speed, both of which show a positive relationship. The domain-averaged seafloor warming also decreases with the typhoon's translation speed. Moreover, there exists a positive correlation between the domain-averaged sea surface cooling and seafloor warming. The different mechanisms that caused the seafloor warming for the 12 typhoons were also investigated in this study.

Keywords: typhoon; Zhejiang coastal waters; HYCOM reanalysis data; oceanic response



Citation: Pan, Y.; Cao, A.; Wu, Y.; Lu, S.; Fan, L.; Li, P. On the Response of Zhejiang Coastal Waters to 12 Typhoons from 2011 to 2015. *J. Mar. Sci. Eng.* **2022**, *10*, 543. <https://doi.org/10.3390/jmse10040543>

Academic Editor: Efim Pelinovsky

Received: 18 March 2022

Accepted: 12 April 2022

Published: 14 April 2022

Publisher's Note: MDPI stays neutral with regard to jurisdictional claims in published maps and institutional affiliations.



Copyright: © 2022 by the authors. Licensee MDPI, Basel, Switzerland. This article is an open access article distributed under the terms and conditions of the Creative Commons Attribution (CC BY) license (<https://creativecommons.org/licenses/by/4.0/>).

1. Introduction

The Northwest Pacific Ocean is the region with the highest concentration of tropical cyclones (typhoons) around the world [1]. China is located to the west of the Northwest Pacific Ocean and has a long coastline. There are many typhoons landing on the southeastern coast of China per year, which cause severe damages. Given that there are many coastal facilities and marine ranches in the coastal waters of China, understanding the oceanic response to typhoons is of great importance.

Typhoons are a powerful weather system that has strong dynamical and thermal effects on the ocean as they pass over. Typhoons import a large amount of energy into the ocean in a short period through momentum exchange at the air–sea interface, causing strong near-inertial waves (NIWs) and turbulent mixing. This process can be divided into the forcing stage and relaxation stage. In the forcing stage, the wind stress of typhoons is strong, and the action time ranges from half a day to a day, which will induce NIWs [2–5]. In the relaxation stage, the NIWs caused by typhoons propagate to the deep ocean [6–9]. In terms of thermal response, a significant effect of typhoons on the ocean is the cooling of sea surface temperature (SST) and the warming of subsurface temperature (it is manifested as seafloor warming in coastal waters) [10]. There are three main processes through which typhoons cause SST cooling: turbulent mixing, advection (mainly upwelling), and air–sea heat exchange [11]. Both observations and numerical simulations suggest that nearly 75–90% of typhoon-induced SST cooling is attributed to the turbulent mixing at the bottom of the mixed layer, which brings the relatively colder water to the sea surface [12].

As part of the East China Sea, the Zhejiang coastal waters are frequently affected by typhoons. However, due to the lack of in situ observations, our knowledge about the response of Zhejiang coastal waters to typhoons is limited. Several previous studies [13–15] have reported that the hybrid coordinate ocean model (HYCOM) reanalysis data can reasonably reproduce the oceanic response to typhoons. Therefore, the HYCOM reanalysis results were adopted in this study to investigate the dynamical and thermal response of Zhejiang coastal waters to the 12 typhoons from 2011 to 2015, and the relationship between oceanic response and typhoon characteristics was revealed based on statistics, aiming to deepen our understanding of regional ocean dynamics. The paper is organized as follows. The HYCOM reanalysis data and corresponding data analysis methods are introduced in Section 2. The main results are presented in Section 3. Finally, a summary completes the paper in Section 4.

2. Data and Methods

2.1. Typhoons

We selected 12 typhoons that passed over Zhejiang coastal waters from 2011 to 2015 for research. They are Meari and Muifa in 2011; Khunan, Haikui, Tembin and Bolaven in 2012; Leepi and Kongrey in 2013; Neoguri, Nakri and Fungwong in 2014; Chanhom in 2015. The time that they passed over Zhejiang coastal waters was mainly from June to September. Among them, Haikui, Fungwong and Chanhom landed on the Zhejiang coast. During the period in Zhejiang coastal waters (27–33°N, 120–130°E), Chanhom and Meari had the largest and smallest averaged maximum wind speeds, which were 43.33 and 12.82 m/s, respectively. The paths of the 12 typhoons are shown in Figure 1. Detailed information about the 12 typhoons is listed in Table 1. These data are available from the Tropical Cyclone Data Center of the China Meteorological Administration [16,17] (<http://tcdata.typhoon.org.cn>, accessed on 1 September 2021).

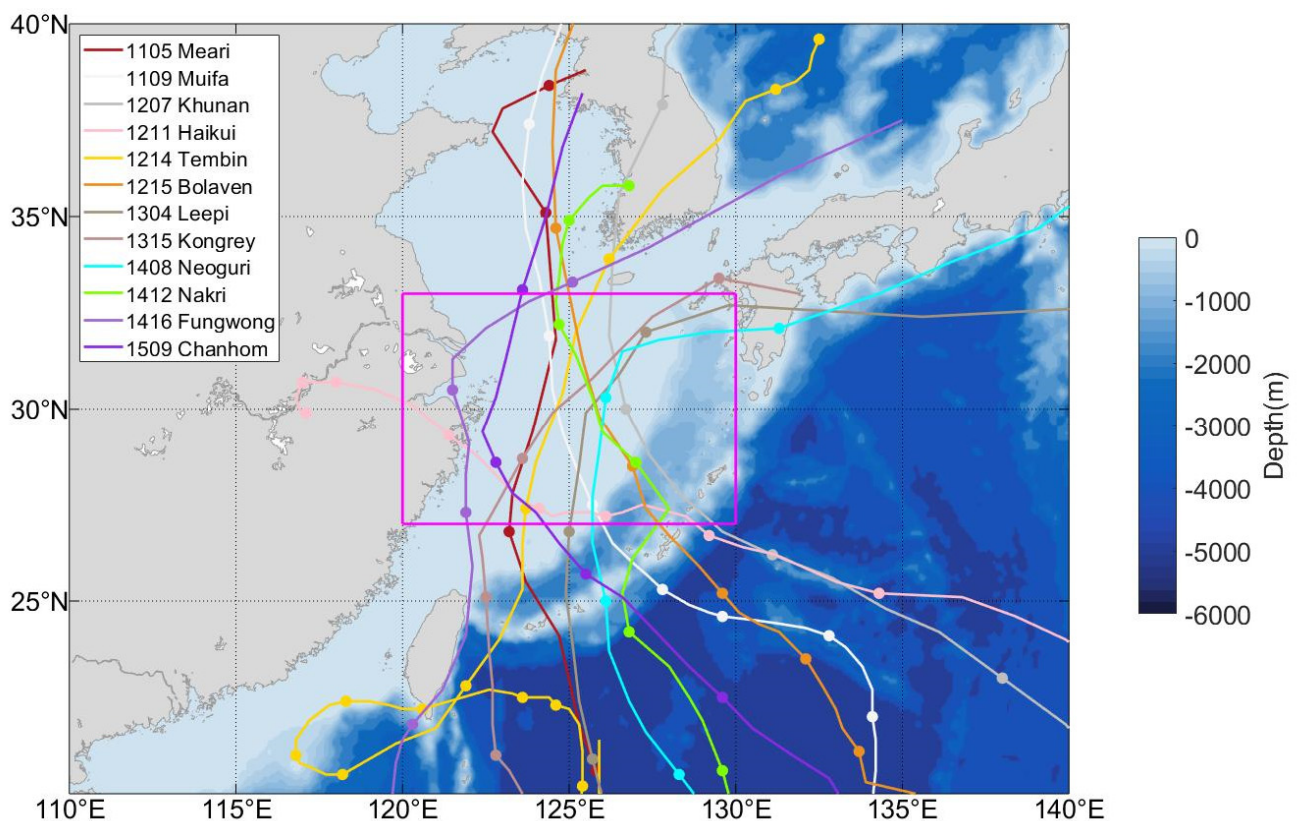


Figure 1. Bathymetry of the East China Sea and tracks of the 12 typhoons. The magenta box denotes the study domain, Zhejiang coastal waters.

Table 1. Detailed information of the 12 typhoons. Note that the maximum wind speed and translation speed are the averaged values in the study domain.

Number	Name	Entry Time to the Study Domain	Maximum Wind Speed (m/s)	Translation Speed (m/s)
1105	Meari	25/06/2011	28.67	12.82
1109	Muifa	06/08/2011	34.6	6.29
1207	Khunan	17/07/2012	24	8.33
1211	Haikui	05/08/2012	33.08	3.74
1214	Tembin	29/08/2012	29.5	8.84
1215	Bolaven	27/08/2012	42	7.74
1304	Leepi	20/06/2013	16.8	11.48
1315	Kongrey	30/08/2013	17.8	8.83
1408	Neoguri	08/07/2014	37.33	6.82
1412	Nakri	01/08/2014	23.71	5.08
1416	Fungwong	22/09/2014	21.5	4.98
1509	Chanhom	10/07/2015	43.33	5.52

2.2. HYCOM Reanalysis Data

The HYCOM reanalysis data (version: GLBu0.08/expt_53.X), including horizontal velocities, water temperature and salinity in Zhejiang coastal waters (27–33°N, 120–130°E) were used to analyze the oceanic response to the 12 typhoons. These data have a spatial resolution of 1/12.5° and a temporal interval of 3 h, which are vertically divided into 40 uneven layers. These data were downloaded from <https://www.hycom.org/dataserver/gofs-3pt1/reanalysis> (accessed on 1 September 2021).

2.3. Satellite-Observed SST Data

The satellite-observed SST data during the passage of the 12 typhoons in the Zhejiang coastal waters were downloaded from the Remote Sensing Systems (<http://www.remss.com>, accessed on 1 September 2021) and compared with the HYCOM reanalysis data. These data have a spatial resolution of 1/4° and a temporal interval of 1 day. Appendix A shows the comparison between the satellite-observed and HYCOM SST, which validates the reasonability of the HYCOM reanalysis data.

2.4. Methodology

The power spectrum analysis of horizontal velocity during each typhoon's transit period showed that there is a significant peak near the local inertial frequency. Although the local inertial frequency is close to those of diurnal tides in Zhejiang coastal waters, the peak near the local inertial frequency corresponds to typhoon-induced NIWs, because the HYCOM reanalysis results (version: GLBu0.08/expt_53.X) do not contain tidal forcing. According to the result of power spectrum analysis, the fourth-order Butterworth filter with cutoff frequencies of (0.77,1.03) cpd (0.79–1.05 times the local inertial frequency) was adopted to extract NIWs from the HYCOM reanalysis data.

To estimate the strength of typhoon-induced NIWs, the near-inertial kinetic energy (NIKE) was calculated as:

$$E = \frac{1}{2} \rho_0 (u^2 + v^2) \quad (1)$$

where $\rho_0 = 1024 \text{ kg/m}^3$ is the reference density, and u and v are the zonal and meridional near-inertial velocities, respectively. The depth-integrated NIKE was also calculated in this study.

Typhoons usually cause strong turbulent mixing in the ocean. To evaluate the intensity of turbulent mixing, the gradient Richardson number (Ri) was calculated:

$$Ri = \frac{N^2}{\left(\frac{du}{dz}\right)^2 + \left(\frac{dv}{dz}\right)^2} \quad (2)$$

where N is the Brunt-Väisälä frequency and is calculated as:

$$N^2 = -\frac{g}{\rho_0} \frac{\partial \rho}{\partial z} \tag{3}$$

where $g = 9.8 \text{ m/s}^2$ is the acceleration due to gravity, and ρ and z are the density and depth of seawater. Generally, $Ri < 1/4$ is regarded as the criterion for shear instability [18,19]. In this study, we first interpolated the velocities and densities onto uniform 5-m levels and then calculated the Ri at each level. The proportion of shear instability ($Ri < 1/4$) in the upper 50 m was used to assess the intensity of turbulent mixing.

Since the HYCOM does not provide vertical velocity, it is diagnosed by calculating the divergence of horizontal velocities according to the continuity equation of the incompressible fluid [20]:

$$\frac{\partial w}{\partial z} = -\left(\frac{\partial u}{\partial x} + \frac{\partial v}{\partial y}\right) \tag{4}$$

Assuming that w at the seafloor is zero, we can estimate the direction of vertical velocity in the water column according to the divergence of horizontal velocities. If the divergence of horizontal velocities is always positive (negative) in the water column, w is negative (positive), which indicates the occurrence of downwelling (upwelling).

3. Results

3.1. Dynamical and Thermal Response of Zhejiang Coastal Waters to Typhoon Muifa in 2011

The dynamical and thermal response of Zhejiang coastal waters to typhoon Muifa in 2011 was shown as an example. Figure 2a,c displays the raw zonal and meridional velocities of the HYCOM reanalysis data at (29.2°N, 128.7°E). Before Muifa passed, the background velocity of the upper ocean in the East China Sea was relatively weak, with an amplitude of less than 0.5 m/s; after the passage of Muifa, the velocity of the upper ocean gradually increased and a fluctuation signal appeared. Around 8 August, the velocity amplitude was about 0.7–1 m/s.

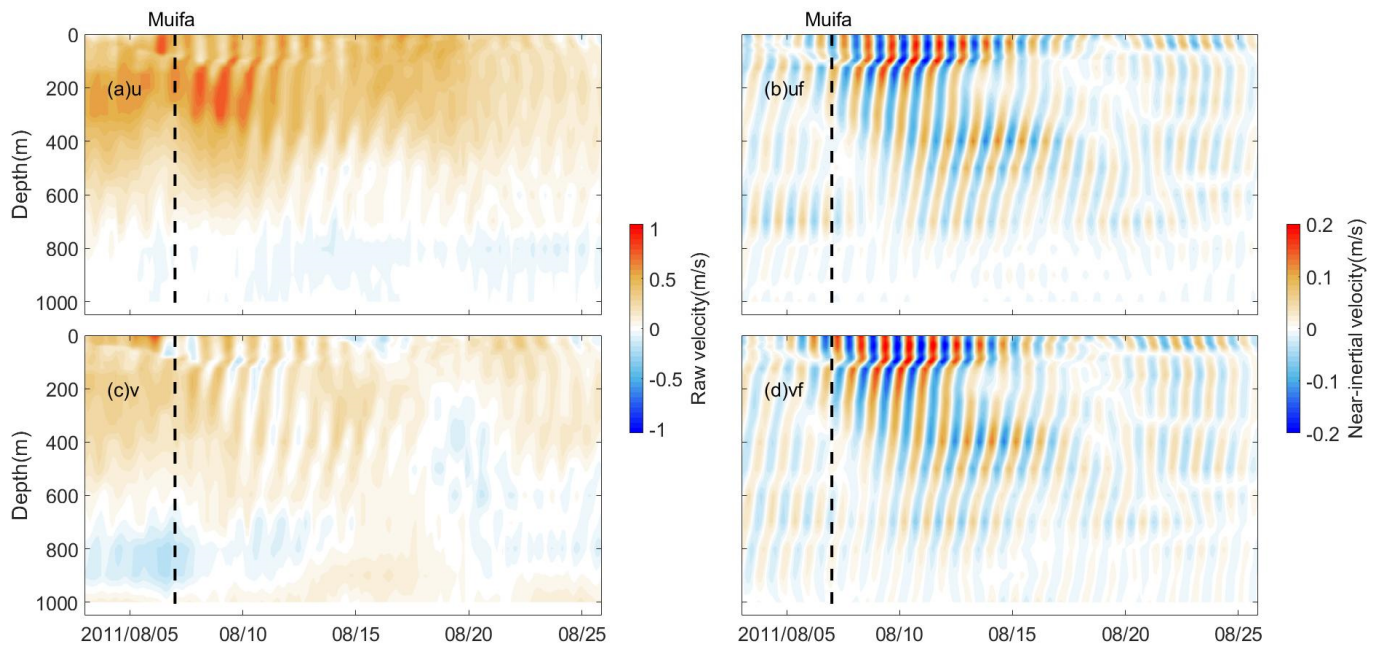


Figure 2. (a,b) Zonal and (c,d) meridional velocities of (a,c) raw HYCOM reanalysis data and (b,d) filtered NIWs as a function of time and depth. The vertical dashed line in each subfigure denotes the time when Muifa passed.

As shown in Figure 2b,d, Muifa induced NIWs at (29.2°N, 128.7°E) on 6 August, which gradually increased and reached the maximum (~0.2 m/s) around 11 August. The phase of Muifa-induced NIWs had an obvious pattern of upward propagation, which means that the vertical group speed was downward. In other words, the NIKE induced by Muifa propagated downward to the deep ocean. As shown in Figure 2, Muifa-induced NIWs could reach ~800 m depth several days after its passage.

Figure 3 shows the depth-integrated NIKE at 00:00 from 5 to 19 August with an interval of two days. On 5 August, Muifa-induced NIKE had appeared in this domain before Muifa entered. Muifa left the domain on 7 August, but the NIKE continuously increased until 11 August and reached the maximum of 6 kJ/m². Then, the NIKE gradually dissipated. On 19 August, the NIKE was almost on the same level as that on 5 August. Moreover, it was found that the NIKE was significant where the water depth is greater than 300 m.

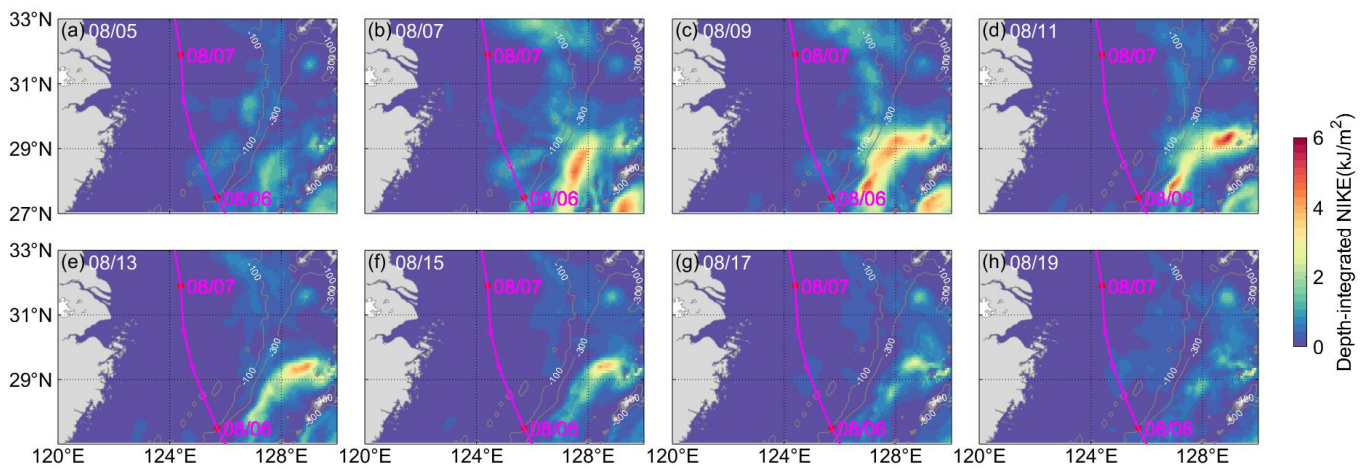


Figure 3. Depth-integrated NIKE at 00:00 on (a) 5, (b) 7, (c) 9, (d) 11, (e) 13, (f) 15, (g) 17 and (h) 19 August. In each subfigure, the magenta curve denotes the track of Muifa and the gray curves represent the 100 and 300 m isobaths.

Zhejiang coastal waters not only had a dynamical response to Muifa but also exhibited a thermal response. Figure 4 shows the SST at 00:00 from 3 to 14 August with an interval of one day. Before Muifa entered the area on 3 August, the SST of the whole area was relatively high (26–32 °C). On 5 and 6 August, slight SST cooling appeared. On 7 August when Muifa left the area, significant SST cooling appeared to the north of 31°N with the minimum SST lower than 22 °C. With time going on, the SST cooling was enhanced. Until 14 August, significant SST cooling was still easily detected in the domain. To the north of 31°N, the maximum SST cooling was approximately −9 °C, whereas to the south of 31°N, the maximum SST cooling was approximately −4 °C.

Figure 5 shows the seafloor temperature at 00:00 from 3 to 14 August, with an interval of one day. Before Muifa entered the area on 3 August, the seafloor temperature varied within a wide range from 0 to 30 °C. Due to the deep bathymetry, the seafloor temperature in the sea of 27–31°N and 127–130°E was about 0–10 °C. As the water depth becomes shallower, the seafloor became warmer. When Muifa entered the area on 6 August, the seafloor temperature of Zhejiang coastal waters became slightly warmer. Muifa left the area on 7 August, and the seafloor temperature in the area of 27–33°N and 122–124°E showed a significant increase. On 7 August, the seafloor warming reached a maximum of about 10 °C. Similar phenomenon has been reported in the area to the north of the Yangtze River [21].

3.2. Correlation between the Oceanic Response of Zhejiang Coastal Waters and Typhoon Characteristics

Figure 6 shows the NIKE of the 12 typhoons in the Zhejiang coastal waters. Note that because typhoons Tembin and Bolaven were too close in time, we did not separate them. Strong NIKE was induced during each typhoon’s transit. For each typhoon (or double

typhoons Tembin and Bolaven), the strongest NIKE appeared to the right of the typhoon's track and the NIKE was significant where the water depth is greater than 300 m. Among the 12 typhoons, Neoguri caused the strongest NIKE (Figure 6h), followed by Tembin and Bolaven (Figure 6e) and Chanhom (Figure 6k), of which the maximum intensity was 45 kJ/m^2 , 25 kJ/m^2 and 25 kJ/m^2 , respectively. In contrast, the NIKE caused by the other typhoons was relatively small, mostly below 10 kJ/m^2 .

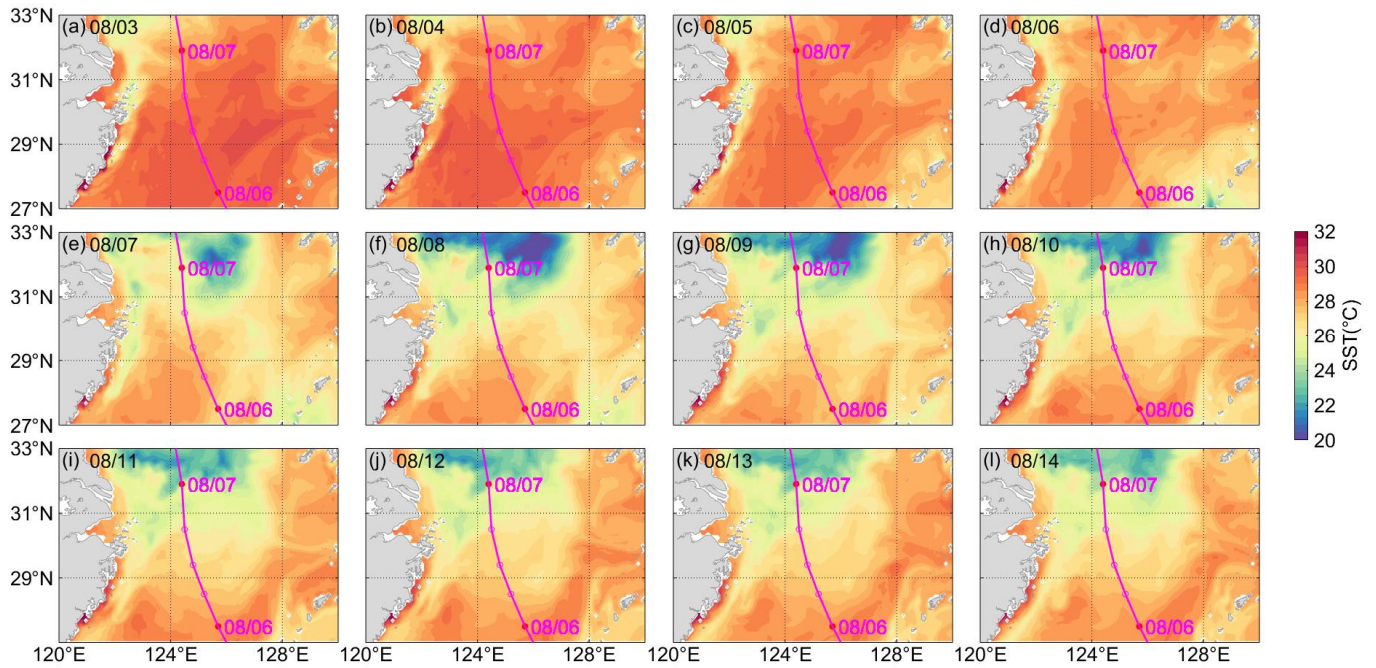


Figure 4. SST at 00:00 on (a) 3, (b) 4, (c) 5, (d) 6, (e) 7, (f) 8, (g) 9, (h) 10, (i) 11, (j) 12, (k) 13 and (l) 14 August.

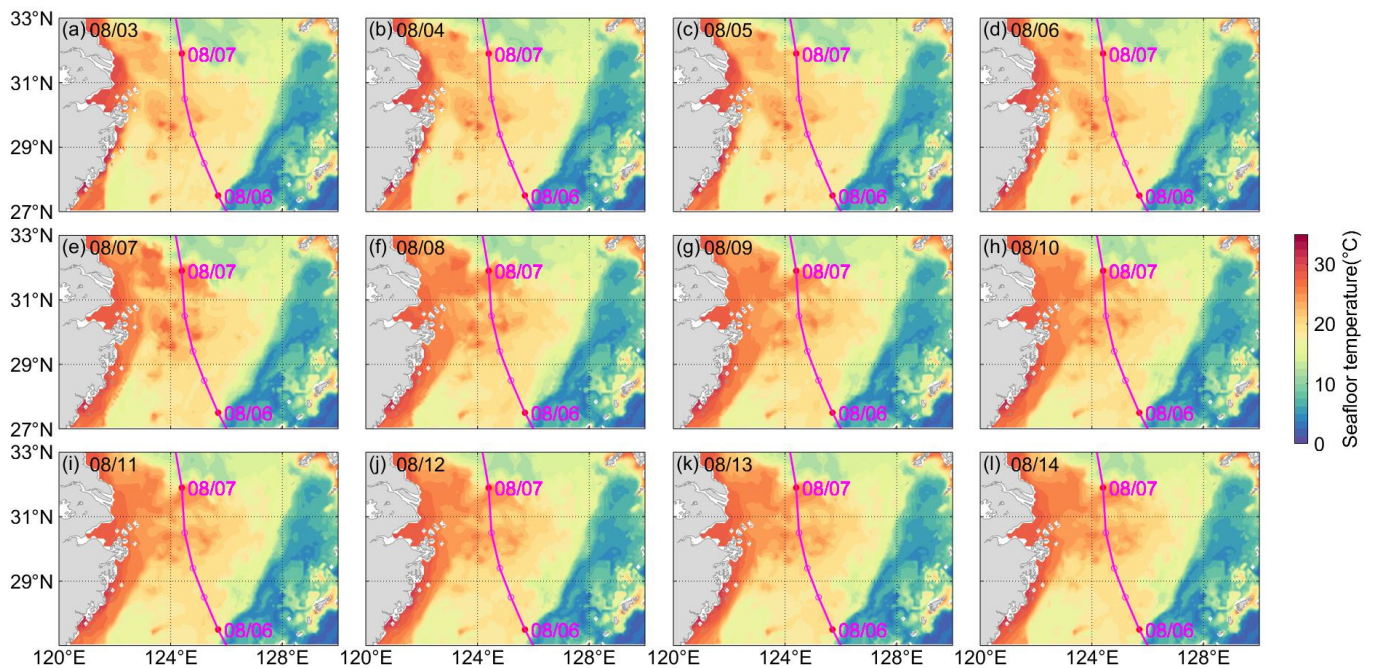


Figure 5. Same as Figure 4 but for seafloor temperature. Seafloor temperature at 00:00 on (a) 3, (b) 4, (c) 5, (d) 6, (e) 7, (f) 8, (g) 9, (h) 10, (i) 11, (j) 12, (k) 13 and (l) 14 August.

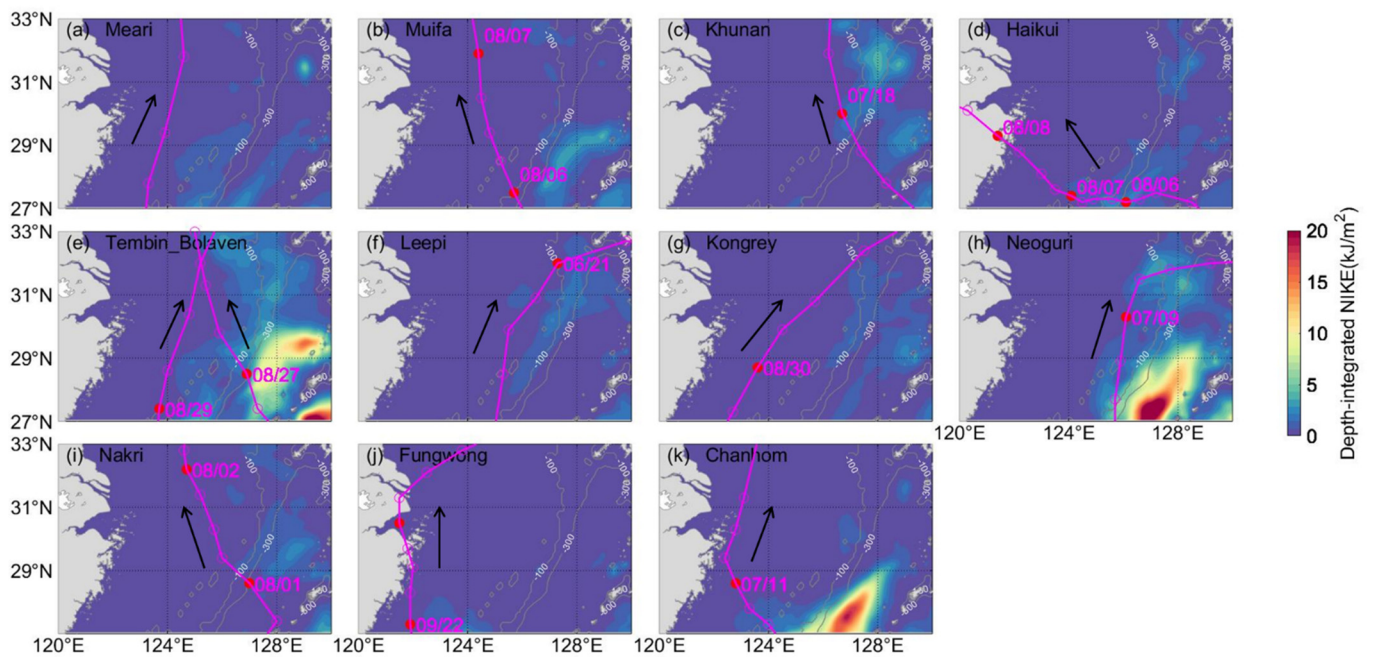


Figure 6. The NIKE was averaged in the 7 days after the passage of the typhoon. The black arrow(s) in each subfigure denotes the moving direction of the typhoon(s).

Figure 7 shows the SST cooling of Zhejiang coastal waters caused by the 12 typhoons, which was calculated as the difference between the minimum SST within seven days after the passage of the typhoon and the SST before the typhoon. Among the 12 typhoons, Muifa caused the maximum SST cooling (Figure 7b), followed by Tembin and Bolaven (Figure 7e), of which the maximum SST cooling was $-9\text{ }^{\circ}\text{C}$ and $-8\text{ }^{\circ}\text{C}$, respectively. In contrast, the SST cooling caused by the other typhoons was relatively small, mostly above $-4\text{ }^{\circ}\text{C}$. For most typhoons (or double typhoons Tembin and Bolaven), the maximum SST cooling appeared to the right of the typhoon’s track, but for Khunan and Kongrey, which have small values of the maximum wind speed (Table 1), the maximum SST cooling appeared to the left of the typhoon’s track.

Figure 8 shows the seafloor warming caused by the 12 typhoons, which was calculated as the difference between the maximum seafloor temperature within seven days after the passage of the typhoon and the seafloor temperature before the typhoon. The seafloor warming caused by the 12 typhoons was within $10\text{ }^{\circ}\text{C}$. Muifa caused the maximum seafloor warming (Figure 8b), which was followed by Haikui (Figure 8d). Although the characteristics of the 12 typhoons (Table 1) and the SST cooling caused by the 12 typhoons (Figure 8) are different, the seafloor warming patterns induced by the 12 typhoons show a common feature: the seafloor warming was remarkable in the shallow waters near the Zhejiang coast.

Figure 9 shows the correlation between the aforementioned oceanic response of the Zhejiang coastal waters and typhoon characteristics, including the maximum wind speed and translation speed (Table 1). The SST cooling, seafloor warming and NIKE were averaged in the whole domain. From Figure 9a, it is easy to detect an obvious positive correlation between the SST cooling and the maximum wind speed, the same as [11]. In contrast, there is no significant change in the SST cooling with the increase of the typhoon’s translation speed (Figure 9b), which suggests that there is no obvious correlation between them. As shown in Figure 9c, the seafloor warming shows an increasing trend with the maximum wind speed, which suggests a positive correlation between them. In contrast, the seafloor warming decreases with the increase of typhoon’s translation speed (Figure 9d), indicating a negative correlation. As for the NIKE, it is clearly shown in Figure 9e that the NIKE becomes stronger with the increase of the maximum wind speed, whereas its

relationship with the typhoon's translation speed is not obvious (Figure 9f). Moreover, the seafloor warming is also found to be positively correlated with the SST cooling (Figure 10).

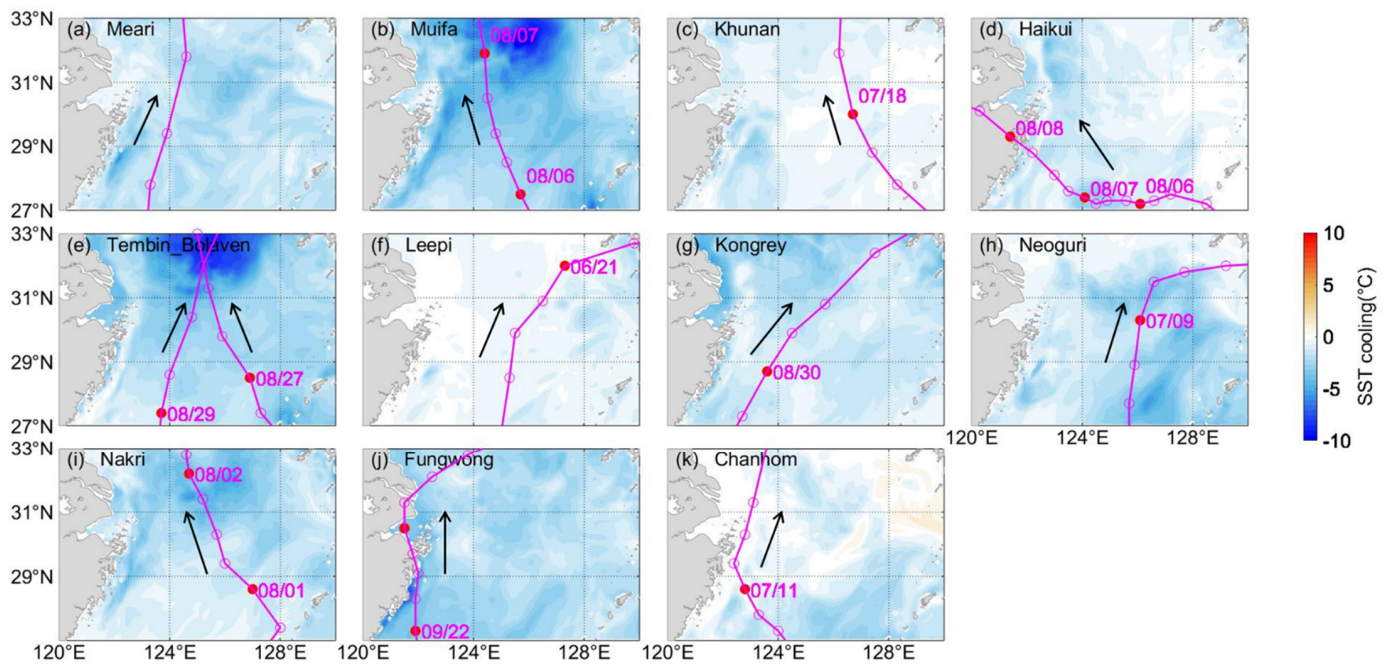


Figure 7. SST cooling of Zhejiang coastal waters caused by the 12 typhoons. The black arrow(s) in each subfigure denotes the moving direction of the typhoon(s).

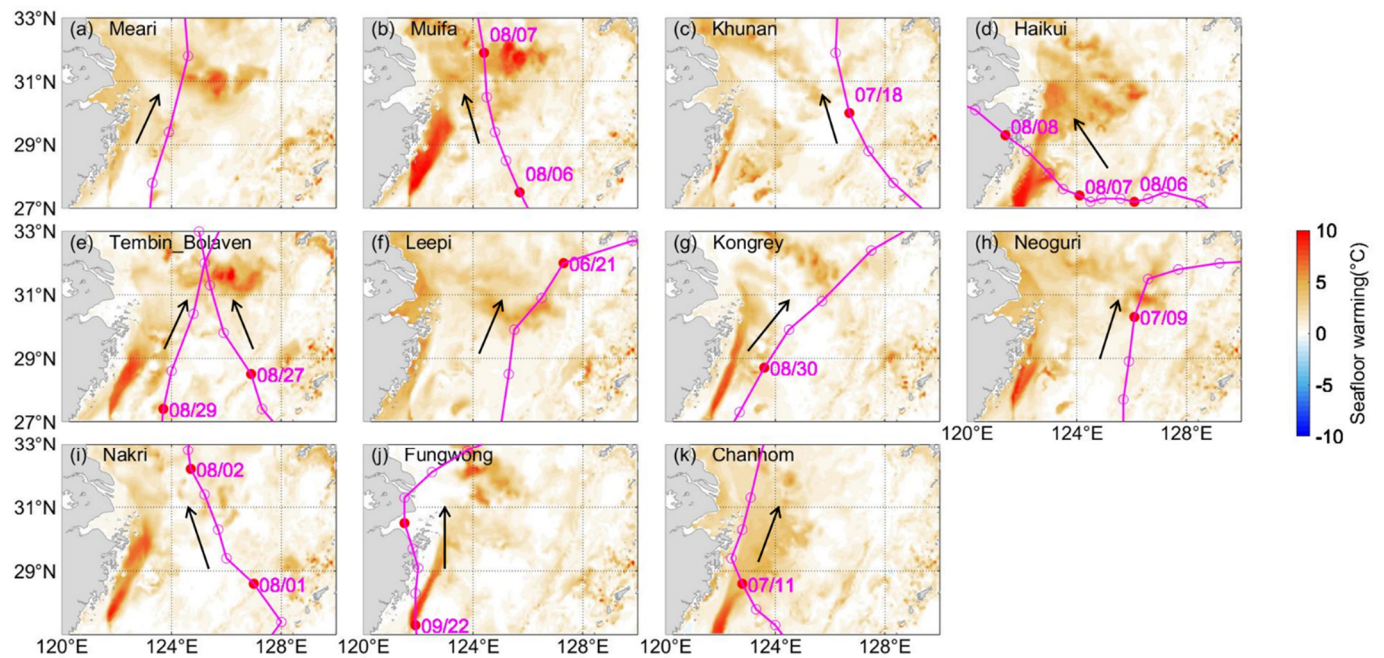


Figure 8. Seafloor warming of Zhejiang coastal waters caused by the 12 typhoons. The black arrow(s) in each subfigure denotes the moving direction of the typhoon(s).

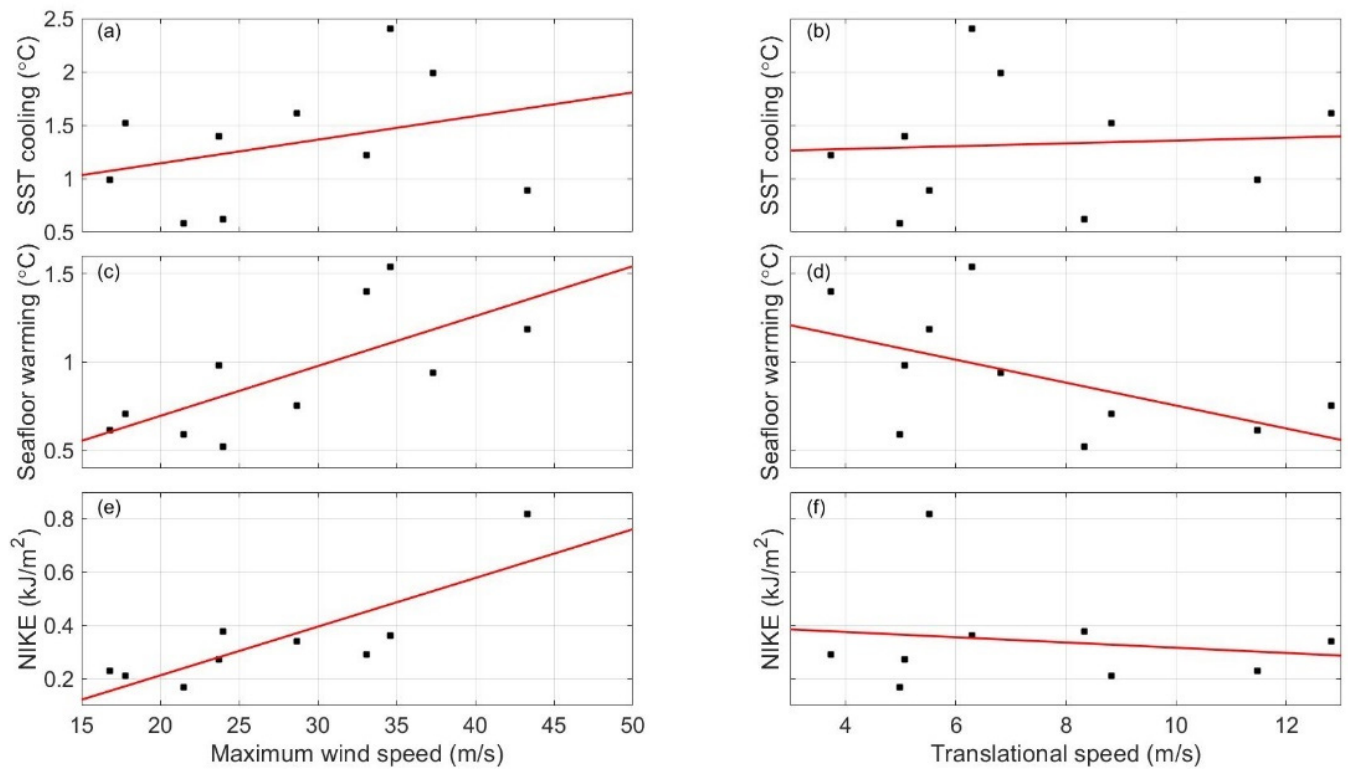


Figure 9. Scatter plots of the (a,b) SST cooling, (c,d) seafloor warming, and (e,f) NIKE versus (a,c,e) the maximum wind speed and (b,d,f) translation speed. Note that the results corresponding to typhoons Tembin and Bolaven are not shown, because they are too close in time (Table 1) to separate their individual influence on the SST cooling, seafloor warming, and NIKE. The red line in each subfigure denotes the linear fitting result. Note that because the NIKE caused by typhoon Neoguri is extremely high, it is not shown in (e,f) and is not considered in the fitting or correlation calculation.

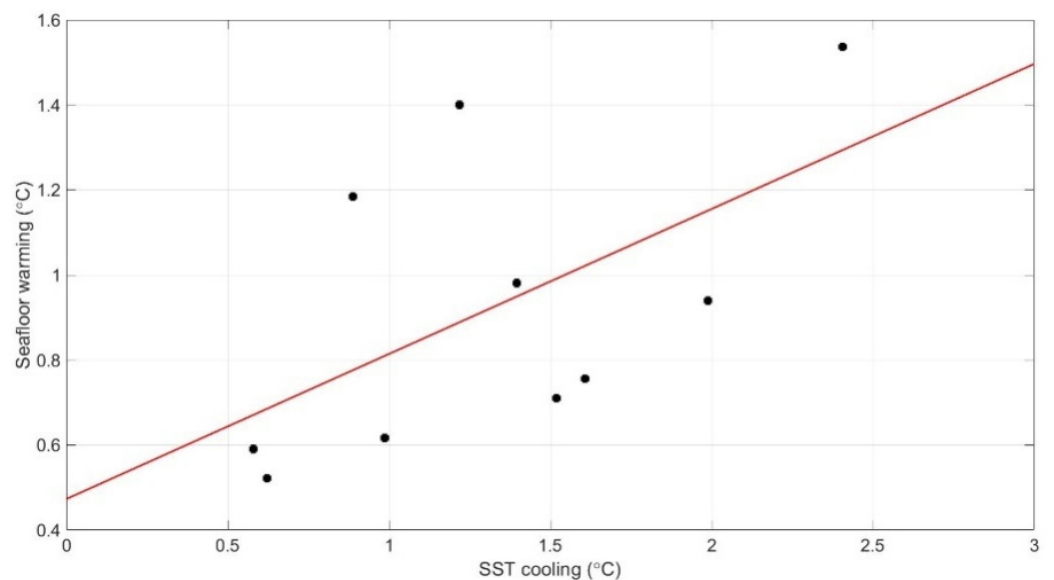


Figure 10. Scatter plots of the seafloor warming versus SST cooling. Note that the results corresponding to typhoons Tembin and Bolaven are not shown. The red line denotes the linear fitting result.

To study the significance of correlations between the oceanic response and typhoon characteristics, the corresponding correlation coefficients and p -values were calculated and are listed in Table 2. It is generally considered that a small value of p (usually smaller than 0.05) means a significant correlation. As shown in Table 2, the correlation coefficient between the seafloor warming (NIKE) and the maximum wind speed is 0.70 (0.83) and the corresponding p -value is 0.02 (0.01), which means that the seafloor warming (NIKE) is significantly positively correlated with the maximum wind speed. The p -value between the seafloor warming and typhoon’s translation speed (SST cooling) is 0.10 (0.08), which is only a little larger than 0.05, suggesting that the correlation between the seafloor warming and typhoon’s translation speed (SST cooling) is generally acceptable, combined with the results shown in Figures 9 and 10. The correlation coefficient between the seafloor warming and typhoon’s translation speed (SST cooling) is -0.54 (0.57), indicating a negative (positive) correlation between them. As for other correlations, the p -values are much greater than 0.05, indicating that these correlations are insignificant. These results are generally consistent with the results shown in Figures 9 and 10.

Table 2. Correlation coefficients and p -values (in the bracket) between the oceanic response (SST cooling, seafloor warming and NIKE) and typhoon characteristics (the maximum wind speed and translation speed).

	SST Cooling (°C)	Seafloor Warming (°C)	NIKE (kJ/m ²)
Maximum wind speed (m/s)	0.33 (0.35)	0.70 (0.02)	0.83 (0.01)
Translational speed (m/s)	0.07 (0.85)	-0.54 (0.10)	-0.16 (0.68)
Seafloor warming (°C)	0.57 (0.08)	-	-

It is generally recognized that both typhoon intensity and translation speed have impacts on the oceanic response, e.g., [22,23]. However, neither the NIKE nor the SST cooling in Zhejiang coastal waters shows a significant correlation with the typhoon’s translation speed (Figure 9 and Table 2). We speculated that a possible cause is that the influence of the typhoon’s translation speed is not isolated from other typhoon characteristics (e.g., typhoon intensity) and the influence of typhoon intensity on the oceanic response may be greater than that of the typhoon’s translation speed in Zhejiang coastal waters.

3.3. Mechanisms of the Seafloor Warming in the Shallow Waters near the Zhejiang Coast

The oceanic turbulent mixing, advection and air-sea heat exchange control the SST cooling [11,12], of which the first two processes can also contribute to the seafloor warming. Attention was first paid to the influence of turbulent mixing on the seafloor warming. Generally, $Ri < 1/4$ is regarded as the criterion for shear instability and occurrence of turbulent mixing [18,19]. Therefore, the proportion of shear instability ($Ri < 1/4$) in the upper 50 m was used to assess the intensity of turbulent mixing in this study.

Figure 11 shows the proportions of shear instability in the upper 50 m during the passage of typhoon Muifa as an example. It is clearly shown that when Muifa entered the study domain at 00:00 on 6 August (Figure 11a), strong turbulent mixing was found as the proportion of shear instability was nearly 100% at most of the area. Note that the proportion of shear instability in the typhoon eye was very small. This phenomenon lasted to 06:00 on 7 August when Muifa’s center reached the northern boundary of the study domain (Figure 11f). Thereafter, the turbulent mixing decreased gradually. After 00:00 on 8 August, the proportion of shear instability in the upper 50 m at most areas was smaller than 40%. These results confirm the occurrence of enhanced turbulent mixing induced by typhoon Muifa.

Figure 12 shows the proportions of shear instability in the upper 50 m for the 12 typhoons. It is clearly shown that for most typhoons (Muifa, Tembin, Bolaven, Neoguri, Nakri, Fungwong and Chanhom), strong turbulent mixing with the proportion of shear instability close to 100% appeared in the shallow waters near Zhejiang coast. For the other typhoons, the proportion of shear instability in the shallow waters near Zhejiang coast was much

smaller. Specially, for typhoons Khunan and Leepi (Figure 12c,f), the proportion of shear instability in the shallow waters near Zhejiang coast was almost 0, which suggests that no enhanced turbulent mixing was caused by the two typhoons near Zhejiang coast. However, typhoons Khunan and Leepi indeed caused seafloor warming (Figure 8c,f), although it was almost the weakest among the 12 typhoons. This result suggests that in addition to the turbulent mixing, the advection (mainly downwelling) may play a role in the seafloor warming. Actually, according to the tracks of Khunan and Leepi, there existed north winds near the Zhejiang coast during the passage of the two typhoons. Given that the Zhejiang coast is nearly south-north, there should exist downwelling near the Zhejiang coast during the passage of Khunan and Leepi, according to the traditional Ekman theory. Figure 13 shows the divergence of horizontal velocities at (28°N, 121.76°E) during the passage of Khunan and Leepi. The water depth at the point is 20 m. It is clearly shown that after the passage of Khunan and Leepi, there exists a period (several days) in which the divergence of horizontal velocities in the whole water column was positive. According to Equation (4), it can be deduced that the vertical velocity in the water column in this period was negative, given that the vertical velocity was zero at the seafloor. In other words, downwelling appeared in this period, which accounts for the seafloor warming (Figure 13c,d). Actually, downwelling was also found for the other typhoons near the Zhejiang coast, which are not shown. Based on the above analysis, we can conclude that, for most typhoons in the Zhejiang coast waters, both typhoon-induced turbulent mixing and downwelling contribute to the seafloor warming; whereas for Khunan in 2012 and Leepi in 2013, the typhoon-induced turbulent mixing was not significant, and the seafloor warming was mostly related to downwelling.

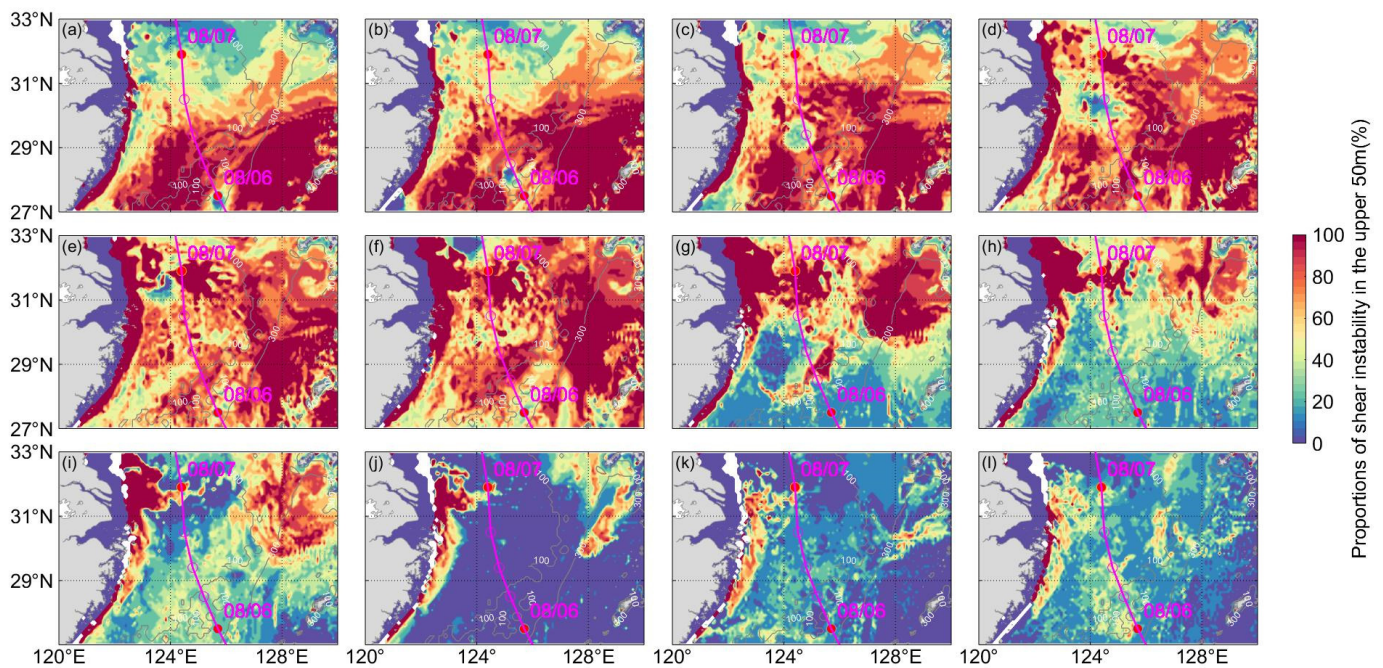


Figure 11. Proportions of shear instability in the upper 50 m induced by typhoon Muifa from (a–l) 00:00 on 6 August to 18:00 on 8 August with an interval of 6 h.

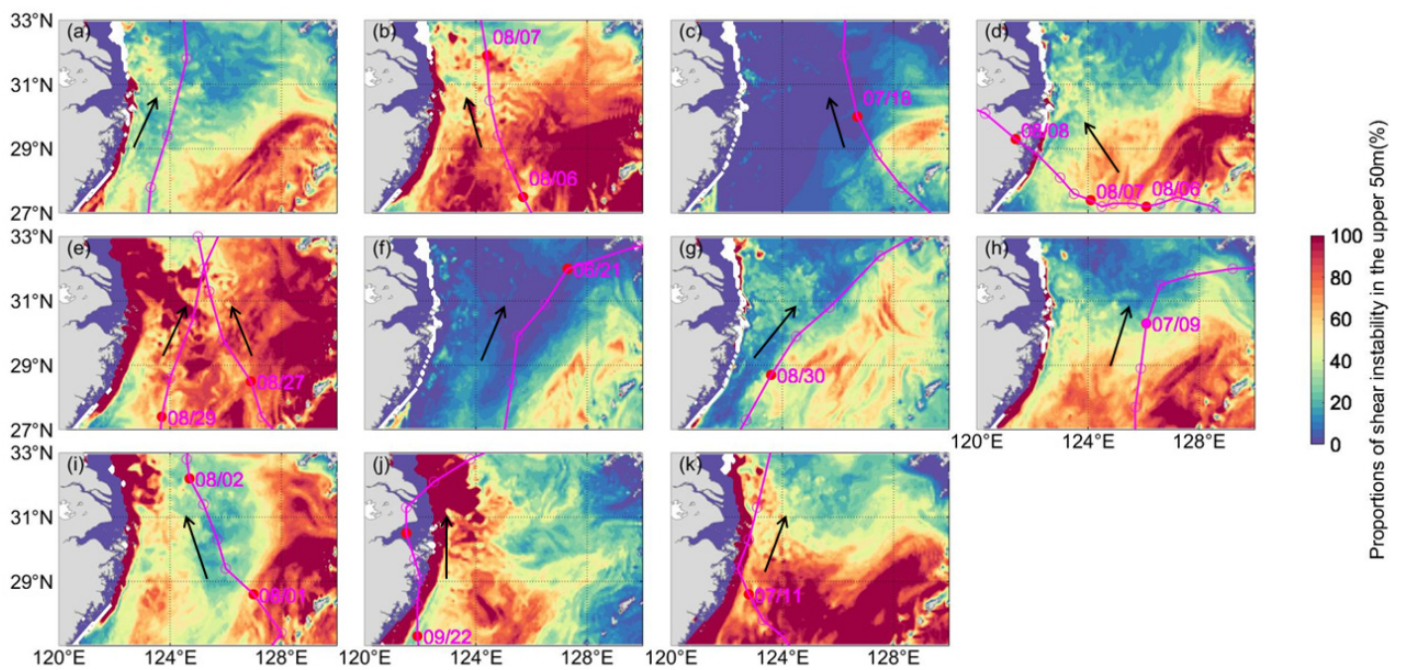


Figure 12. Proportions of shear instability in the upper 50 m induced by (a) Meari, (b) Muifa, (c) Khunan, (d) Haikui, (e) Tembin and Bolaven, (f) Leepi, (g) Kongrey, (h) Neoguri, (i) Nakri, (j) Fungwong and (k) Chanhom. Note that the proportion is averaged in the 1 day after the passage of the typhoon. The black arrow(s) in each subfigure denotes the moving direction of the typhoon(s).

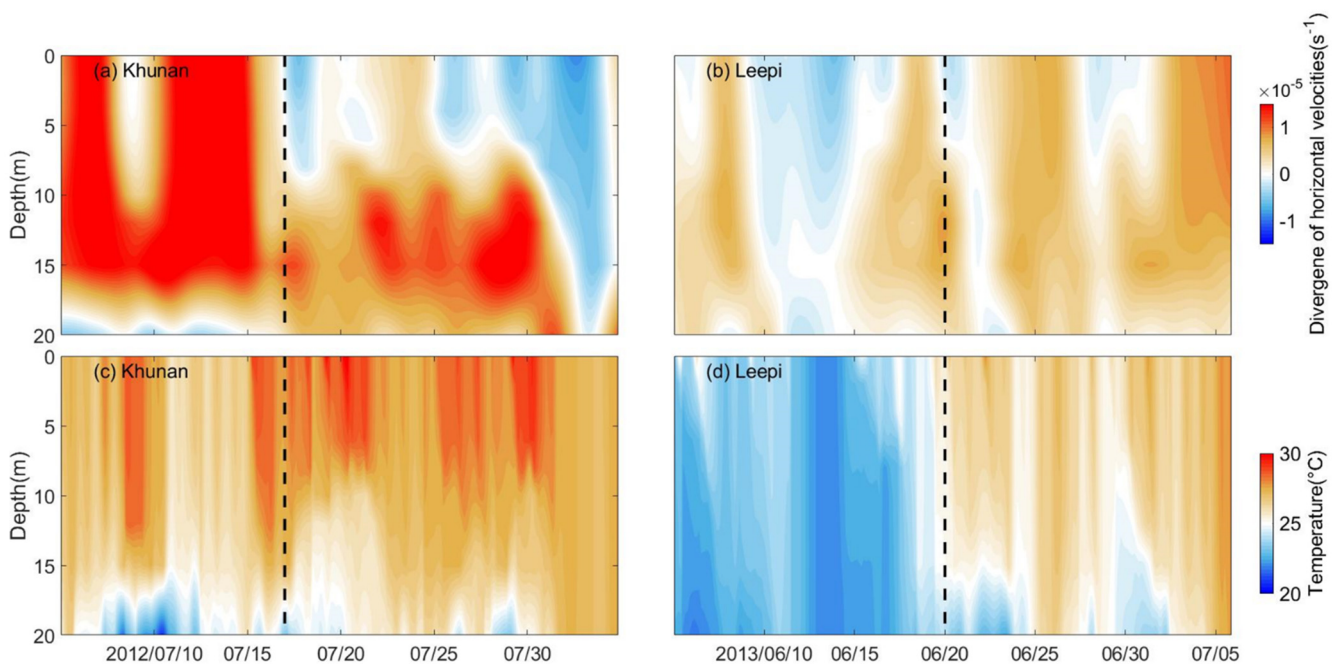


Figure 13. (a,b) Divergence of horizontal velocities and (c,d) water temperature at (28°N, 121.76°E) for (a,c) Khunan and (b,d) Leepi. In each subfigure, the vertical dashed line denotes the time when the typhoon passed.

4. Summary

Based on the HYCOM reanalysis data, the dynamical and thermal responses of the Zhejiang coastal waters to the 12 typhoons (Meari and Muifa in 2011; Khunan, Haikui, Tembin and Bolaven in 2012; Leepi and Kongrey in 2013; Neoguri, Nakri and Fungwong in 2014; Chanhom in 2015) were investigated in this study. Results indicate that all the

12 typhoons caused SST cooling, seafloor warming and NIKE. However, due to the different characteristics, the oceanic response of the Zhejiang coastal waters to the 12 typhoons was different. The SST cooling caused by the typhoons ranged from -9 to -1 °C, and the seafloor warming from 3 to 10 °C. For most typhoons, significant SST cooling appeared to the right of the typhoon's track, whereas the maximum SST cooling caused by Khunan and Kongrey was to the left of their tracks. In contrast, the seafloor warming caused by the 12 typhoons had a common feature, i.e., the seafloor warming was remarkable in the shallow waters near the Zhejiang coast. As for the typhoon-induced NIKE, large values were found to the right of the typhoon's track and in the region where the water depth is greater than 300 m.

To further understand the oceanic response of the Zhejiang coastal waters to typhoons, the correlation coefficients and corresponding *p*-values between the oceanic response (domain-averaged SST cooling, seafloor warming and NIKE) and typhoon characteristics (typhoon's maximum wind speed and translation speed) were calculated. Results indicate that the domain-averaged NIKE and seafloor warming are significantly positively correlated with the typhoon's maximum wind speed. The domain-averaged seafloor warming is also correlated with the typhoon's translation speed, but show a decreasing trend. Moreover, the domain-averaged seafloor warming is found to be correlated with the domain-averaged SST cooling, although their spatial patterns showed large differences.

In this study, the mechanisms to cause seafloor warming were also discussed. It is found that for most typhoons, the seafloor warming was caused by the combined effects of typhoon-induced turbulent mixing and downwelling. However, typhoons Khunan in 2012 and Leepi in 2013 did not cause strong turbulent mixing near the Zhejiang coast and downwelling was found to account for the seafloor warming caused by the two typhoons.

Because of the lack of in situ observations, we believe that the results of this study can deepen our understanding of the oceanic response of Zhejiang coastal waters to typhoons to some extent. Moreover, given that there are many marine ranches near the Zhejiang coast and some of the farmed fish and shellfish are sensitive to water temperature, the results of this study may be useful for the site selection and protection of the marine ranches.

Author Contributions: Conceptualization, A.C.; methodology, Y.P.; formal analysis, Y.P.; writing—original draft preparation, Y.P.; writing—review and editing, A.C., Y.P., Y.W., S.L. and L.F.; supervision, A.C. and P.L.; funding acquisition, A.C. All authors have read and agreed to the published version of the manuscript.

Funding: This research was funded by the Zhejiang Provincial Natural Science Foundation (grant number: LY21D060005), the National Key Research and Development Program of China (grant number: 2019YFD0901305) and the Joint Project of Zhoushan Municipality and Zhejiang University (grant number: 2019C81060).

Conflicts of Interest: The authors declare no conflict of interest.

Appendix A. Comparison between the Satellite-Observed and HYCOM SST

Figure A1 shows the Muifa-induced SST cooling maps from HYCOM reanalysis data and satellite observations. On the whole, the HYCOM SST cooling is generally consistent with that from satellite observations; the maximum SST cooling appeared to the right of Muifa's track and the maximum SST cooling was approximately -9 °C. Figure A2 displays the comparison of domain-averaged SST cooling between HYCOM reanalysis results and satellite observations for the 10 typhoons except for Tembin and Bolaven. For most typhoons, the difference between the HYCOM and satellite-observed SST cooling was small and within ± 0.5 °C. Only for the two typhoons (Muifa and Fungwong), the difference was larger than ± 1 °C. This discrepancy is probably attributed to a combined effect of the lack of tidal forcing and inaccuracy of wind field used in HYCOM. Note that the temporal intervals of HYCOM reanalysis data (3 h) and satellite observations (1 day) are different, which may be a cause for the discrepancy. Based on the aforementioned

results, we think that the HYCOM reanalysis data can reasonably reproduce the thermal response of Zhejiang coastal waters to most typhoons and hence can be used in this study.

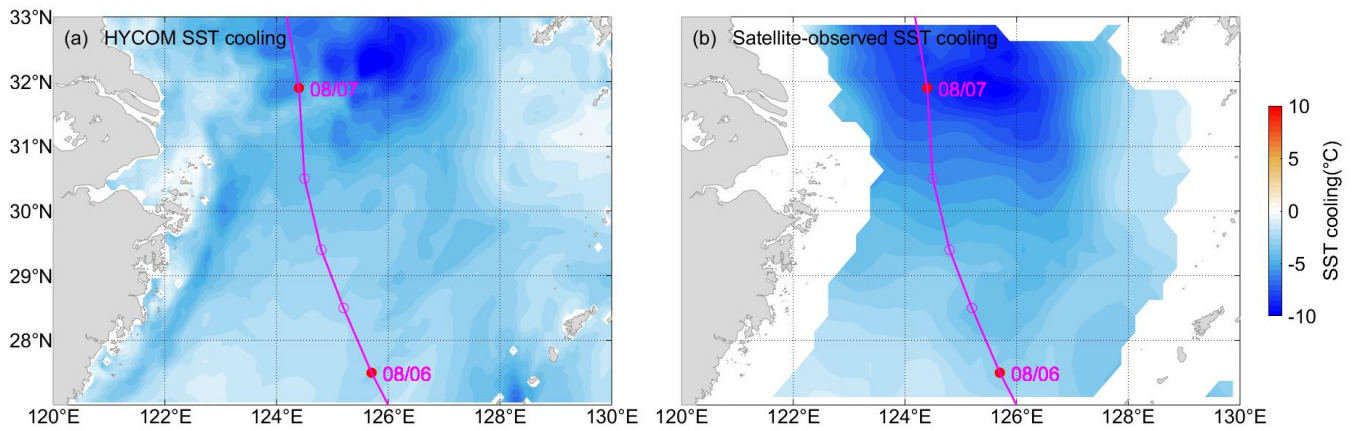


Figure A1. SST cooling caused by typhoon Muifa; (a,b) correspond to the HYCOM reanalysis results and satellite observations, respectively.

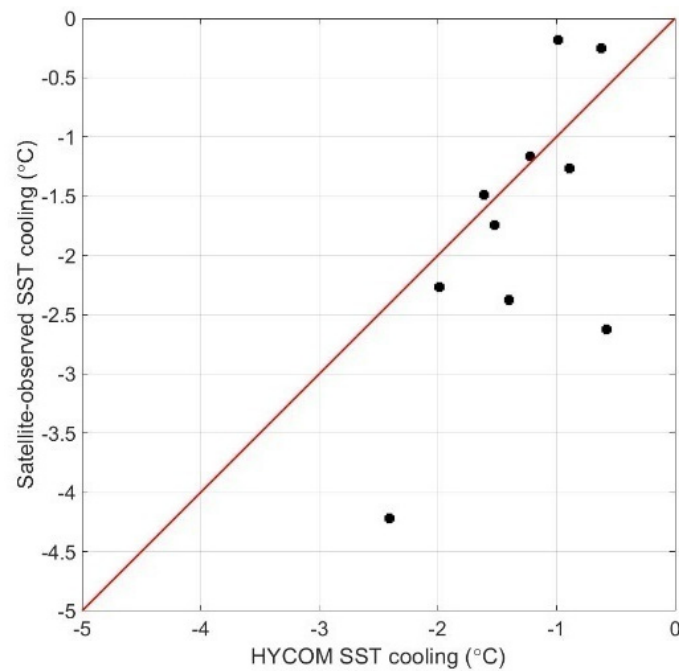


Figure A2. Comparison of the HYCOM and satellite-observed domain-averaged SST cooling. Note that the results corresponding to typhoons Tembin and Bolaven are not shown, because they are too close in time (Table 1) to separate their individual influence on SST cooling.

References

1. D’Asaro, E.; Black, P.; Centurioni, L.; Harr, P.; Jayne, S.; Lin, I.; Lee, C.; Morzel, J.; Mrvaljevic, R.; Niiler, P.P.; et al. Typhoon-Ocean Interaction in the Western North Pacific: Part 1. *Oceanography* **2011**, *24*, 24–31. [[CrossRef](#)]
2. Sanford, T.B.; Black, P.G.; Haustein, J.R.; Feeney, J.W.; Forristall, G.Z.; Price, J.F. Ocean Response to a Hurricane. Part 1: Observations. *J. Phys. Oceanogr.* **1987**, *17*, 2065–2083. [[CrossRef](#)]
3. Sanford, T.B.; Price, J.F.; Girton, J.B. Upper-Ocean Response to Hurricane Frances (2004) Observed by Profiling Em-Apex Floats. *J. Phys. Oceanogr.* **2011**, *41*, 1041–1056. [[CrossRef](#)]
4. Sanford, T.B.; Price, J.F.; Girton, J.B.; Webb, D.C. Highly Resolved Observations and Simulations of the Ocean Response to a Hurricane. *Geophys. Res. Lett.* **2007**, *34*, 5. [[CrossRef](#)]
5. Shay, L.K.; Mariano, A.J.; Jacob, S.D.; Ryan, E.H. Mean and near-Inertial Ocean Current Response to Hurricane Gilbert. *J. Phys. Oceanogr.* **1998**, *28*, 858–889. [[CrossRef](#)]

6. Brooks, D.A. The Wake of Hurricane Allen in the Western Gulf of Mexico. *J. Phys. Oceanogr.* **1983**, *13*, 117–129. [[CrossRef](#)]
7. Dasaro, E.A. Upper-Ocean Inertial Currents Forced by a Strong Storm.2. Modeling. *J. Phys. Oceanogr.* **1995**, *25*, 2937–2952. [[CrossRef](#)]
8. Dasaro, E.A. Upper-Ocean Inertial Currents Forced by a Strong Storm.3. Interaction of Inertial Currents and Mesoscale Eddies. *J. Phys. Oceanogr.* **1995**, *25*, 2953–2958. [[CrossRef](#)]
9. Shay, L.K.; Elsberry, R.L. Near-Inertial Ocean Current Response to Hurricane Frederic. *J. Phys. Oceanogr.* **1987**, *17*, 1249–1269. [[CrossRef](#)]
10. Zhang, H.; He, H.L.; Zhang, W.Z.; Tian, D. Upper Ocean Response to Tropical Cyclones: A Review. *Geosci. Lett.* **2021**, *8*, 1–12. [[CrossRef](#)]
11. Price, J.F. Upper Ocean Response to a Hurricane. *J. Phys. Oceanogr.* **1981**, *11*, 153–175. [[CrossRef](#)]
12. Guan, D.S.; Zhao, W.; Sun, L.; Zhou, C.; Liu, Z.; Hong, X.; Zhang, Y.H.; Tian, J.W.; Hou, Y.J. Tropical Cyclone-Induced Sea Surface Cooling over the Yellow Sea and Bohai Sea in the 2019 Pacific Typhoon Season. *J. Mar. Syst.* **2021**, *217*, 103509. [[CrossRef](#)]
13. Cao, Z.A.; Guo, Z.; Pan, Y.H.; Song, J.B.; He, H.L.; Li, P.L. Near-Inertial Waves Induced by Typhoon Megi (2010) in the South China Sea. *J. Mar. Sci. Eng.* **2021**, *9*, 440. [[CrossRef](#)]
14. Li, J.; Xu, J.X.; Liu, J.L.; He, Y.H.; Chen, Z.W.; Cai, S.Q. Correlation of near-Inertial Wind Stress in Typhoon and Typhoon-Induced Oceanic near-Inertial Kinetic Energy in the Upper South China Sea. *Atmosphere* **2019**, *10*, 17. [[CrossRef](#)]
15. Yang, B.; Hu, P.; Hou, Y.J. Observed near-Inertial Waves in the Northern South China Sea. *Remote Sens.* **2021**, *13*, 3223. [[CrossRef](#)]
16. Lu, X.; Yu, H.; Ying, M.; Zhao, B.K.; Zhang, S.; Lin, L.M.; Bai, L.N.; Wan, R.J. Western North Pacific Tropical Cyclone Database Created by the China Meteorological Administration. *Adv. Atmos. Sci.* **2021**, *38*, 690–699. [[CrossRef](#)]
17. Ying, M.; Zhang, W.; Yu, H.; Lu, X.Q.; Feng, J.X.; Fan, Y.X.; Zhu, Y.T.; Chen, D.Q. An Overview of the China Meteorological Administration Tropical Cyclone Database. *J. Atmos. Ocean. Technol.* **2014**, *31*, 287–301. [[CrossRef](#)]
18. Howard, L.N. Note on a Paper of John W. Miles. *J. Fluid Mech.* **1961**, *10*, 509–512. [[CrossRef](#)]
19. Miles, J.W. On the Stability of Heterogeneous Shear Flows. *J. Fluid Mech.* **1961**, *10*, 496–508. [[CrossRef](#)]
20. Pedlosky, J. *Geophysical Fluid Dynamics*, 2nd ed.; Springer: Berlin/Heidelberg, Germany, 1987.
21. Yang, B.G.; Lu, L.G.; Zhuang, Z.P.; Xiong, X.J.; Wang, G.S.; Guo, Y.L.; Yu, L.; Ma, D.J. Cruise Observation of Shallow Water Response to Typhoon Damrey 2012 in the Yellow Sea. *Cont. Shelf Res.* **2017**, *148*, 1–8. [[CrossRef](#)]
22. Zhao, H.; Tang, D.; Wang, Y. Comparison of phytoplankton blooms triggered by two typhoons with different intensities and translation speeds in the South China Sea. *Mar. Ecol. Prog. Ser.* **2008**, *365*, 57–65. [[CrossRef](#)]
23. Chen, S.; Polton, J.A.; Hu, J.; Xing, J. Local inertial oscillations in the surface ocean generated by time-varying winds. *Ocean. Dyn.* **2015**, *65*, 1633–1641. [[CrossRef](#)]